

## Preparation of ZnO-supported 13X zeolite particles and their antimicrobial mechanism

Mei Li

School of Chemical Engineering and Technology, Guangdong Industry Technical College, Guangzhou 510300, People's Republic of China; Technology Development Center for Polymer Processing Engineering of Guangdong Colleges and Universities, Guangzhou 510300, People's Republic of China; and Advance Technology Development Center for Polymer Processing Engineering of Guangdong, Guangzhou 510300, People's Republic of China

Lijun Wu, Zishou Zhang, and Kancheng Mai<sup>a)</sup>

Materials Science Institute, School of Chemistry, Sun Yat-sen University, Guangzhou 510275, People's Republic of China; Key Laboratory of Polymeric Composites and Functional Materials of Ministry of Education, Guangzhou 510275, People's Republic of China; and Guangdong Provincial Key Laboratory of High Performance Resin-based Composites, Guangzhou 510275, People's Republic of China

(Received 12 June 2017; accepted 2 October 2017)

To improve the antimicrobial properties of ZnO, ZnO-supported 13X zeolite (X-ZnO) was prepared via the facile chemical method. Antimicrobial activities of X-ZnO and ZnO were tested against Gram-negative (*Escherichia coli*) and Gram-positive (*Staphylococcus aureus*) bacteria. X-ZnO showed noticeable antimicrobial activities against *E. coli* and *S. aureus* under visible light conditions, especially against *E. coli*. The minimum inhibitory concentration (MIC) of X-ZnO against *E. coli* was 0.12–0.24 mg/mL. However, there were still much bacteria alive in the nano-ZnO suspensions at the same concentration. To elucidate the antimicrobial activities of X-ZnO, the average concentration of the total reactive oxygen species (ROS) and Zn<sup>2+</sup> ions released from X-ZnO and nano-ZnO were quantitatively analyzed. The obtained results indicated that the average concentration of ROS produced by supported ZnO was much higher than that of nano-ZnO. And the released Zn<sup>2+</sup> ions from X-ZnO and nano-ZnO suspensions were much lower than the MIC of Zn<sup>2+</sup>. Thus, it is believed that the production of ROS in X-ZnO and nano-ZnO suspensions resulted in the difference of antibacterial activities.

### I. INTRODUCTION

Antimicrobial agents can be broadly classified into two types, organic compounds and inorganic materials. Organic antimicrobial agents have broad source, and quick and efficient antimicrobial properties, but their applications are limited due to their sensitivity to high temperature and pressures.<sup>1</sup> Inorganic antimicrobial agents attract much attention due to their safe, nontoxic, and stable properties.<sup>2,3</sup> Inorganic antimicrobial agents mainly include metal particles and metal-oxide particles, such as copper, silver, TiO<sub>2</sub>, ZnO, and so on.<sup>4,5</sup>

Many reports revealed that ZnO showed antimicrobial activities against Gram-positive and Gram-negative bacteria.<sup>6–13</sup> Moreover, it is found that the antimicrobial activities of ZnO were strongly influenced by its size and morphology.<sup>11,14–19</sup> Ohira et al.<sup>11</sup> observed that the antimicrobial activities of ZnO can be improved with diminution of particle size. This was explained due to an increase in the surface area/volume ratio, which resulted in increased generation of H<sub>2</sub>O<sub>2</sub>. Zhang et al.<sup>14</sup> and

Jones et al.<sup>15</sup> also proved improved antimicrobial activities of ZnO against *Escherichia coli* and *Staphylococcus aureus* with diminution of particle size.

To obtain small-particle-size and special-shape ZnO particles, porous materials such as microporous and mesoporous zeolites have been used as host materials due to their high surface area, thermal stability, and ecofriendly nature.<sup>20–24</sup> Recently, Saleh et al.<sup>22–24</sup> prepared zeolite/ZnO and zeolite/ZnO–CuO nanocomposites (NCs) with a type of A-zeolite and found that zeolite/ZnO and zeolite/ZnO–CuO NCs showed remarkable antimicrobial activities. But the antimicrobial activities and the corresponding mechanism of ZnO supported on 13X zeolite (X-ZnO) materials have been little reported.

So far, the exact mechanism for the antimicrobial activities of ZnO particles is still debated. Some reports suggested that the Zn<sup>2+</sup> ions released from ZnO suspension were responsible for the antimicrobial activity,<sup>25–28</sup> whereas some did not.<sup>17,18,29,30</sup> It is generally thought that oxidative stress induced by reactive oxygen species (ROS) generation in the ZnO system is the main mechanism for antibacterial activities.<sup>31–34</sup>

To improve the antimicrobial activities of ZnO and dispersion in polymer matrix, we prepared ZnO-supported

Contributing Editor: Lakshmi Nair

<sup>a)</sup>Address all correspondence to this author.

e-mail: cesmck@mail.sysu.edu.cn

DOI: 10.1557/jmr.2017.410

zeolite with different methods in our previous studies.<sup>35–37</sup> We found that ZnO-supported zeolite-filled polypropylene (PP) or polypropylene random copolymer (PPR) composites have better antimicrobial activities than the same content of nano-ZnO-filled PP or PPR composites. To compare the antimicrobial activities of ZnO and ZnO-supported zeolite and to elucidate the mechanism, the ZnO content, specific surface area, morphology, crystal, element, and optical properties of ZnO supported on the surface of zeolite were characterized with inductively coupled plasma atomic emission spectroscopy, nitrogen adsorption–desorption analyzer, scanning electron microscopy, X-ray diffractometer, and fluorescence spectroscopy. The antimicrobial activities of the supported ZnO and nano-ZnO particles were compared using the optical density (OD) test and plate counting method. The concentration of Zn<sup>2+</sup> ions and ROS ( $\cdot\text{OH}$ ,  $\cdot\text{O}_2^-$ , and  $\text{H}_2\text{O}_2$ ) generation in ZnO solution systems were characterized.

## II. EXPERIMENTAL SECTION

### A. Materials

13X zeolite (X) with an average particle size of about 1  $\mu\text{m}$  and pore diameter about 1.0 nm was supplied by Wuxi Rongdeli Molecular Sieve Factory (Wuxi, China). Zn(NO<sub>3</sub>)<sub>2</sub> (AR), NaOH (AR), concentrated nitric acid (GR), NaCl (AR), HCl (AR), KI (AR), soluble starch (AR), and H<sub>2</sub>O<sub>2</sub> (AR) were bought from Guangzhou Chemical Factory, China. Beef extract (BR) was obtained from Guangdong Huankai Bio-tech Limited Company (Guangzhou, China). Peptone (BR) was provided by Baisai Biological Limited Company (Shanghai, China). Agar (BR) was supplied from Qiyun Bio-tech Limited Company (Guangzhou, China). *E. coli* (ATCC8739) and *S. aureus* (ATCC6538) with the concentration of 10<sup>10</sup> CFU/mL and 10<sup>9</sup> CFU/mL, respectively, were obtained from Guangzhou Institute of Microbiology (Guangzhou, China). Nano-ZnO with an average particle size of about 30 ± 10 nm, terephthalic acid (AR), 2-hydroxyl terephthalic acid, and nitroterazoliumblue chloride (AR) were supplied by Aladdin Chemistry Co. Ltd. (Shanghai, China).

### B. The preparation methods and procedures

20 g of 13X zeolite was pretreated in a muffle furnace for 3 h, then transferred to a 200-mL three-neck flask after the zeolite cooling to room temperature. After the system was evacuated to 0.063 MPa with a vacuum pump and the pressure was kept for 0.5 h to remove air from the flask and hole of zeolite, 60 mL of 20 wt% aqueous solution of zinc nitrate was added into the flask and the mixture was stirred for 1 h. Then 0.5 mol/L of NaOH aqueous solution was added into the system to adjust the pH to 8.0 and stirred for 1 h. The mixture was filtered and

dried at room temperature. The filtered mixture was calcified for 4 h at 300 °C. The prepared sample was denoted as X-ZnO. The schematic is shown in FIG. 1.

## C. Characterization techniques

### 1. Characterization of X-ZnO

The morphology of X, X-ZnO, and nano-ZnO particles was observed with a scanning electron microscope (SEM; SEM-4800, Hitachi, Japan). These samples were gold coated and observed at an acceleration voltage of 20 kV. The ZnO contents on ZnO-supported microporous zeolite were characterized on SPECTRO CIROS VISION (METEK Commercial and Trading Co., Ltd., Shanghai, China) inductively coupled plasma atomic emission spectroscopy. Nitrogen adsorption/desorption isotherms were measured at –196 °C in Micromeritics ASAP 2020 automated gas adsorption system ( $P/P_0 = 0.20$ ). The specific surface area was calculated on a basis of the Brunauer–Emmet–Teller (BET) method from the adsorption branch. The crystal type of nano-ZnO particles and X-ZnO were conducted with a Rigaku Geigerflex Model D/Max-III A rotating anode X-ray diffractometer. The scanning range was 20–70° with a step scanning rate of 10°/min. The fluorescence spectra of X, X-ZnO, and nano-ZnO particles were characterized by fluorescence spectroscopy (RF-5301PC, Shimadzu, Japan) at an excitation wavelength of 320 nm and emission wavelength of 330–800 nm. The slit width of excitation and emission is 10 nm.

### 2. OD growth curve measurement

After LB broth was treated through heat sterilization, a certain amount of X, X-ZnO and nano-ZnO particles was added into the LB broth. Then the bacteria were inoculated to the LB broth. The LB broth containing of inoculated bacteria and X, X-ZnO and nano-ZnO was irradiated by a lamp with the power of 11 W, the irradiation wavelength of 400–700 nm and the irradiation height of 10 cm. Cell growth was monitored by measuring the OD at 595 nm on a microplate reader (iMark, Bio-Rad Laboratories, Inc).

### 3. Determination of viable cell number by plating method

The number of viable cells was determined using the traditional surface plating method.<sup>15,18</sup> Briefly, a 20- $\mu\text{L}$  control (Luria-Bertani [LB] broth and inoculated bacteria without zeolite and ZnO) and cell samples (LB broth, inoculated bacteria with zeolite or ZnO) were serially diluted with 0.9% NaCl solution. The viable cell number in each sample was determined by evenly spreading 20  $\mu\text{L}$  of the dilution onto the LB-agar plate for aerobic incubation at 37 °C. After 24 h, colonies on each plate were counted. All experiments were duplicated three times, and the results were expressed as mean ± standard deviation.

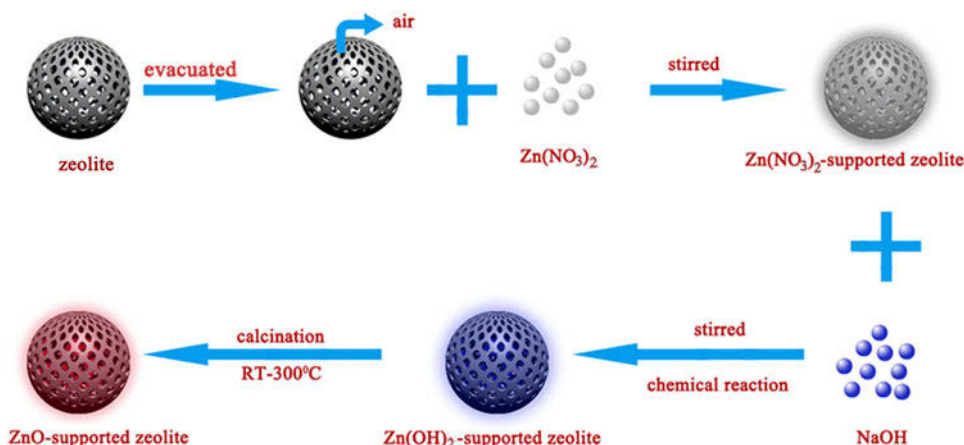


FIG. 1. The formation of X-ZnO.

#### 4. Determination of $\text{Zn}^{2+}$ ions

The aqueous suspensions of X-ZnO and nano-ZnO with the effective ZnO concentration of 0.48 mg/mL were vibrated at 37 °C and 200 rpm for 24 h. The samples were centrifuged at 4000 rpm for 10 min and then filtered with 0.44- $\mu\text{m}$  Millipore membranes. The concentration of  $\text{Zn}^{2+}$  ions in the aqueous suspension was measured using ICP-AES (SPECTRO CIROS VISION, Germany).

#### 5. Determination of $\cdot\text{OH}$

According to reports,<sup>31,38,39</sup> the  $\cdot\text{OH}$  was usually qualitatively analyzed by electron spin resonance (ESR). To quantitatively characterize the production of  $\cdot\text{OH}$  in ZnO aqueous suspensions, chemical methods were used to measure the production of  $\cdot\text{OH}$  in this article. The  $\cdot\text{OH}$  can easily react with terephthalic acid to yield fluorescent 2-hydroxy-terephthalate, which is stable for hours and can readily be assessed using standard fluorimeters. The concentration of  $\cdot\text{OH}$  can be determined from fluorescent intensity at 425 nm in the fluorescence spectra at 312 nm excitation.<sup>19</sup> The suspensions containing ZnO with an effective concentration of 2 g/L and terephthalate with a concentration of  $2 \times 10^{-3}$  mol/L were treated with an ultrasonicator for 10 min in the dark. Then, the suspensions were irradiated as the same as C. Characterization Techniques. 2 with a magnetic stirrer to ensure the homogenization of the suspensions. The suspensions were centrifuged and filtered with 0.44- $\mu\text{m}$  Millipore membrane. The fluorescence spectra of the filtrates containing 2-hydroxy-terephthalate were detected with a fluorescence spectrometer (Perkin Elmer-LS55, Guangzhou Perkin Elmer Instrument Co., Ltd., Guangzhou, China).

#### 6. Determination of $\cdot\text{O}_2^-$

Because the nitrotetrazolium blue chloride (NBT) can easily react with  $\cdot\text{O}_2^-$  to form insoluble purple formazan, the NBT as a trap agent was used to quantitatively

determine the amount of  $\cdot\text{O}_2^-$  generated from the ZnO aqueous suspensions.<sup>38,39</sup> The mixture containing aqueous suspensions of ZnO with a concentration of 2 g/L and the NBT with a concentration of  $5 \times 10^{-5}$  mol/L were treated as the same as C. Characterization Techniques. 5. The content of  $\cdot\text{O}_2^-$  in the mixture was quantitatively analyzed by detecting the decrease in the concentration of NBT in the mixture with ultraviolet-visible (UV-vis) spectrophotometer (Perkin Elmer-Lambda750).

#### 7. Determination of $\text{H}_2\text{O}_2$

$\text{H}_2\text{O}_2$  generated from ZnO suspensions can be determined by UV-vis spectrophotometry with KI and starch.<sup>40</sup> The aqueous suspensions of ZnO with a concentration of 2 g/L were irradiated and treated as the same as 2.3.5. 5 mL of filtrate was added to a 10-mL flask, and then 0.5 mL of NaCl solution (200 g/L), 0.2 mL of HCl (10%), 0.3 mL of KI solution (10 g/L), and 0.2 mL soluble starch solution (10 g/L) were successively dropped into the flask, and finally the flask was brought up to volume with water. The absorbance at 570 nm of the final solution was detected by UV-vis spectrophotometer (Perkin Elmer-Lambda750, Guangzhou Perkin Elmer Instrument Co., Ltd., Guangzhou, China).

### III. RESULTS AND DISCUSSION

#### A. Characterization of X-ZnO

The SEM morphologies of zeolite (X), X-ZnO, and nano-ZnO (as control) particles are depicted in Fig. 2. It can be seen that the surface of X is smooth and the nano-ZnO particles are spherical in shape; the ZnO particles supported on the surface of zeolite is layer-like; and the supported ZnO is coated on the surface of zeolite in the form of a molecular layer. Obviously, the particle size of the supported ZnO is much smaller than that of nano-ZnO (as control). The XRD pattern of X, X-ZnO, and nano-ZnO is shown in Fig. 3(a). The figure shows the

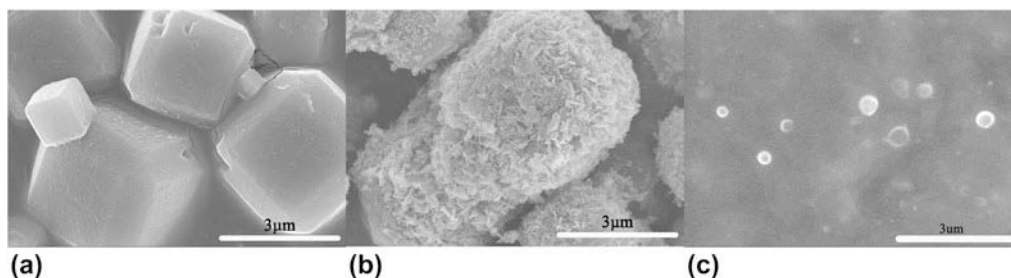


FIG. 2. SEM morphologies of X (a), X-ZnO (b), and nano-ZnO (c) particles.

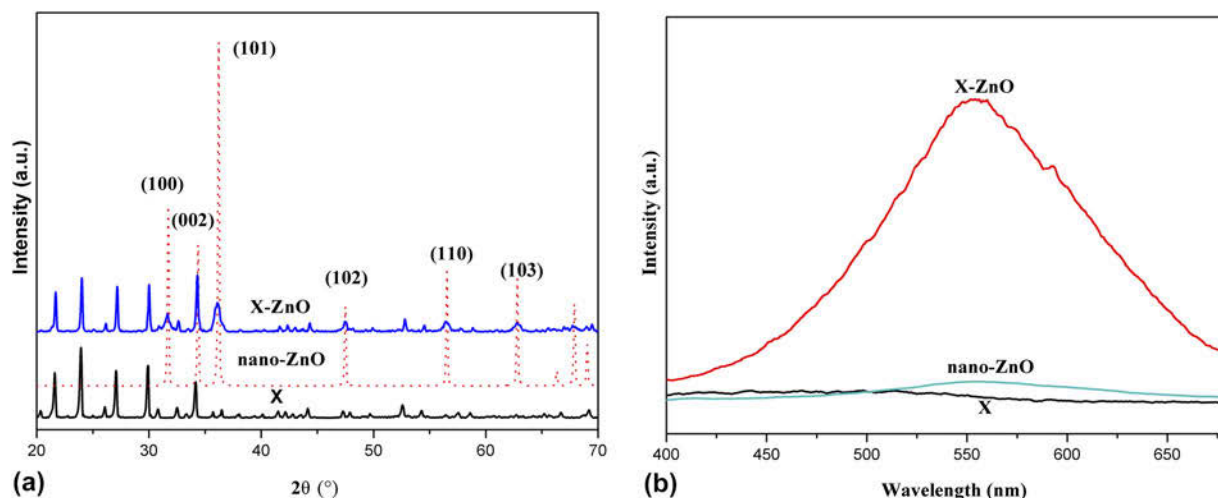


FIG. 3. X-ray diffraction diagram (a) and fluorescence spectra (b) of X, X-ZnO, and nano-ZnO particles.

patterns of zeolite peaks before (X) or after supported ZnO (X-ZnO) was similar, showing that the zeolite structure is stable and did not change. Diffraction peaks at  $31.76$ ,  $34.42$ ,  $36.21$ ,  $47.53$ ,  $56.59$ , and  $62.9^\circ$  are assigned to reflections from the (100), (002), (101), (102), (110), and (103) lattice planes hexagonal wurtzite zinc oxide crystals with reference pattern NO 01-079-2205. It is confirmed that ZnO supported on the surface of zeolite and supported ZnO are hexagonal wurtzite structures.<sup>41</sup> Meanwhile, the results obtained by ICP-AES indicated that the ZnO content in X-ZnO was 24.36%. The BET-specific area of X, X-ZnO, and nano-ZnO are 505.2, 172.6, and 7.8  $\text{m}^2/\text{g}$ , respectively. It is generally considered that the fluorescence spectra of ZnO mainly include near-band-edge emission band at about 380 nm and broad deep-level emission band from 450 to 630 nm.<sup>42</sup> The deep-level emission of ZnO consists of a green emission around 520 nm and a near-yellow emission around 640 nm.<sup>43,44</sup> Although the origin of green emission is controversial,<sup>44-47</sup> it is generally assigned to the singly ionized oxygen vacancies.<sup>46,47</sup> The fluorescence spectra of ZnO supported on the surface of 13X zeolite and nano-ZnO particles are shown in Fig. 3(b). It can be seen that the fluorescence intensity of green emission of X-ZnO is higher than that of nano-ZnO particles. It is indicated that the

oxygen vacancies of ZnO supported on the surface of zeolite is much more than that of nano-ZnO particles. The investigation by Xu et al.<sup>19</sup> suggested that the oxygen vacancies on the surface of ZnO were proportional to the production of  $\text{H}_2\text{O}_2$ . The high oxygen vacancies of ZnO support on the surface of zeolite are expected to result in the production of much more  $\text{H}_2\text{O}_2$ .

## B. The antimicrobial activity of X-ZnO

Figure 4 shows the OD growth curves of *E. coli* in LB broth after being treated with different contents of X, X-ZnO, and nano-ZnO. Generally, the longer the delayed growth time and the lower the OD value, the better the antimicrobial activities. The effective ZnO contents in X-ZnO of 0.125 mg/mL, 0.25 mg/mL, 0.5 mg/mL, 1.0 mg/mL, and 2.0 mg/mL suspensions were 0.03 mg/mL, 0.06 mg/mL, 0.12 mg/mL, 0.24 mg/mL, and 0.48 mg/mL, respectively. It can be observed that the OD values of all samples have no change before 8 h. For being incubated above 8 h, the OD values were obviously different. When the concentration of zeolite was increased from 0.125 mg/mL to 2.0 mg/mL in the suspension, the OD value was decreased from 1.44 to 1.13. It showed that there are no remarkable antimicrobial

activities of zeolite. And when the concentration of nano-ZnO particles was increased from 0.03 mg/mL to 0.48 mg/mL in the suspensions, the OD value was decreased from 1.44 to 0.75, indicating that the nano-ZnO particles have antibacterial activities. For X-ZnO, when the effective ZnO reached 0.24 mg/mL, the OD value was almost zero and the growth time was delayed to 24 h. This result proved that the antimicrobial activities of ZnO support on the surface of zeolite were much better than those of nano-ZnO particles.

To further compare the antimicrobial activities between the ZnO supported on the surface of zeolite and nano-ZnO particles, the loss viability of *E. coli* and *S. aureus* after being treated by X, X-ZnO, and nano-ZnO particles was investigated, and the effect of the concentration of X, X-ZnO, and nano-ZnO particles on the loss of viability of *E. coli* is shown in Fig. 5(a). From Fig. 5(a), it is obvious that the number of viable cells were reduced with increasing effective ZnO contents. When the dose of X-ZnO was 1.0 mg/mL (effective ZnO was 0.24 mg/mL), the viable cell of *E. coli* was reduced to zero. The result showed that the minimum inhibitory concentration (MIC) of X-ZnO against *E. coli* was 0.12–0.24 mg/mL. However,

for nano-ZnO particles, there were still much bacteria alive at the concentration of 0.48 mg/mL. In summary, the antimicrobial activities of X-ZnO were higher than those of nano-ZnO particles. And this result was consistent with the OD test.

For loss viability of *S. aureus*, the experimental results treated by X, X-ZnO, and nano-ZnO particles with effective ZnO concentration of 0.48 mg/mL are shown in Fig. 5(b). It can be observed that 13X zeolite almost has no antimicrobial activities against *S. aureus*. The antimicrobial activities against *S. aureus* are as follows: X-ZnO > nano-ZnO particles. But the antimicrobial activities of X, X-ZnO, and nano-ZnO particles against *E. coli* were much better than that of *S. aureus*. It is attributed to the different structure between *E. coli* and *S. aureus*, and the *S. aureus* has a stronger endurance toward antimicrobial agent than *E. coli*.<sup>1,8,17</sup>

### C. Mechanism of enhanced antimicrobial activities of ZnO

Oxidative stress induced by ROS ( $\cdot\text{OH}$ ,  $\text{H}_2\text{O}_2$ , and  $\text{O}_2^-$ ) generation in the ZnO system is thought to be the main mechanism for their antimicrobial activities.<sup>31–34</sup>

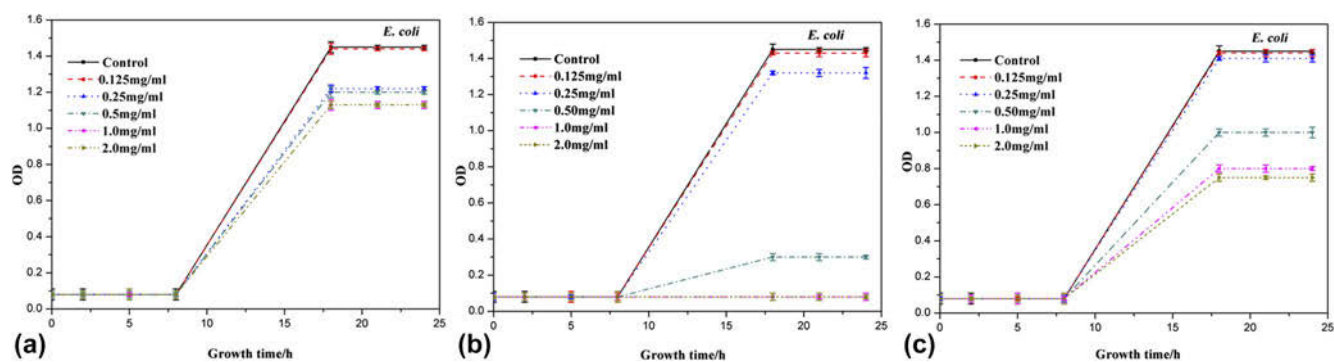


FIG. 4. OD growth curves of *E. coli* in LB broth at 37 °C after the bacterial cells were treated with different contents of X (a), X-ZnO (b), and nano-ZnO (c).

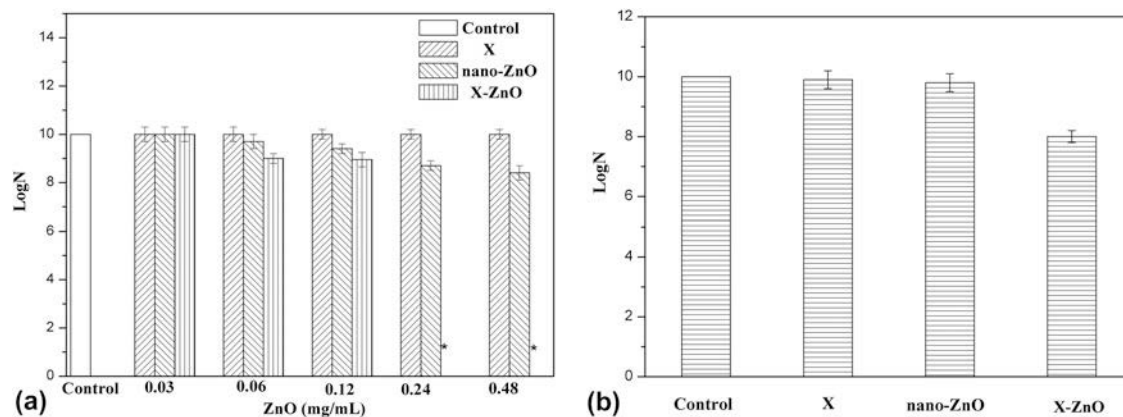


FIG. 5. Antimicrobial activities of X, X-ZnO, and nano-ZnO against *E. coli* (a) and *S. aureus* (b) under visible light conditions. \* represents no colony.

The generation of ROS on the surface of ZnO is as follows<sup>31</sup>: when irradiated by light with photoenergy higher than the band gap of ZnO, the electrons of ZnO are promoted across the band gap to the conduction band to create a hole in the valence band. The electron hole can react with H<sub>2</sub>O molecules in the suspension of ZnO, resulting in the formation of  $\cdot\text{OH}$  and H<sup>+</sup>. In addition, the superoxide anion radicals ( $\text{O}_2^-$ ) can be produced by combination of electrons of ZnO and O<sub>2</sub> molecules dissolved in the suspension and can in turn react with H<sup>+</sup> to generate hydrogen peroxide radicals (HO<sub>2</sub> $\cdot$ ). Subsequently, the HO<sub>2</sub> $\cdot$  collides with electrons to produce hydrogen peroxide anion (HO<sub>2</sub><sup>-</sup>). Thus the HO<sub>2</sub><sup>-</sup> can react with H<sup>+</sup> to produce H<sub>2</sub>O<sub>2</sub> molecules. The produced  $\cdot\text{OH}$ , H<sub>2</sub>O<sub>2</sub>, and  $\text{O}_2^-$  all have strong oxidation for the organic biomolecules. Therefore, ZnO has good antimicrobial activity.

To further understand the different antimicrobial activity of the supported ZnO and nano-ZnO particles, the produced  $\cdot\text{OH}$ , H<sub>2</sub>O<sub>2</sub>, and  $\text{O}_2^-$  in the aqueous suspensions of X-ZnO and nano-ZnO particles were measured, and the average concentration of ROS generation in X-ZnO and nano-ZnO suspensions were compared. It is generally suggested that the intensity of the peak at 425 nm was related to the amount of  $\cdot\text{OH}$  in the ZnO suspensions. It can be seen from Fig. 6(a) that zeolite (X) suspension had no emission peak at 425 nm, and this indicates that the zeolite suspension did not produce  $\cdot\text{OH}$  under visible light irradiation. X-ZnO and nano-ZnO suspension both have emission peaks at 425 nm, which proves that X-ZnO and nano-ZnO suspension could generation  $\cdot\text{OH}$  under visible light conditions. Additionally, the amount of  $\cdot\text{OH}$  produced increased when prolonging irradiation time [Fig. 6(b)].

Because NBT, as the trap agent, can react with  $\text{O}_2^-$  to form purple-blue precipitate, the generation of  $\text{O}_2^-$  can

be quantitatively evaluated from the decrease of NBT concentration in the suspensions of X-ZnO and nano-ZnO particles. Generally speaking, the lower the absorption of NBT, the more that NBT reacted with  $\text{O}_2^-$ , more was the production of  $\text{O}_2^-$  in the suspensions. Figure 7(a) shows the UV-vis absorption spectra of NBT in the suspensions irradiated under visible light conditions for 2 h. It can be seen that the UV-vis absorption spectra of NBT in the zeolite suspension had little change, this indicates that zeolite suspension did not produce  $\text{O}_2^-$  under visible light conditions. The UV-vis absorption intensity of NBT at 259 nm in the suspensions are as follows: nano-ZnO > X-ZnO, indicating that the concentration of  $\text{O}_2^-$  in the suspensions was X-ZnO > nano-ZnO. The production of  $\text{O}_2^-$  in the suspensions irradiated for different times also confirmed that the concentration of  $\text{O}_2^-$  in the suspensions was X-ZnO > nano-ZnO, as shown in Fig. 7(b).

The production of H<sub>2</sub>O<sub>2</sub> in the suspension of zeolite, X-ZnO, and nano-ZnO particles was also investigated. H<sub>2</sub>O<sub>2</sub> can react with KI and starch to form a blue complex with a maximum absorption peak at about 570 nm in the UV-vis absorption. It can be observed from Fig. 8(a) that zeolite suspension has no absorption peak in 570 nm, this indicates that zeolite suspension did not produce H<sub>2</sub>O<sub>2</sub>. And the absorption intensity at about 570 nm of X-ZnO was higher than that for nano-ZnO. And the amount of H<sub>2</sub>O<sub>2</sub> in the suspensions increased with increasing irradiation time [Fig. 8(b)].

Table I summarizes the average concentration of three types of ROS ( $\cdot\text{OH}$ , H<sub>2</sub>O<sub>2</sub>, and  $\text{O}_2^-$ ) for zeolite, X-ZnO, and nano-ZnO particles irradiated for 2 h. It can be seen that zeolite did not produce measurable ROS. The average concentration of total ROS in X-ZnO and nano-ZnO suspensions was 65.24 and 28.87  $\mu\text{mol}$ , respectively. The total ROS produced by X-ZnO was higher than that by nano-ZnO. Obviously, supported

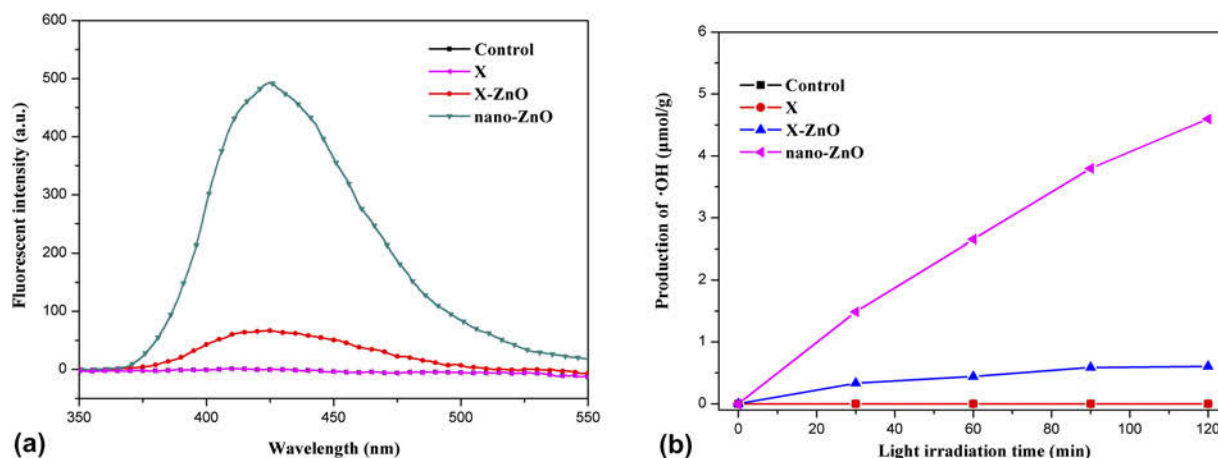


FIG. 6. Production of  $\cdot\text{OH}$  in the suspension of ZnO samples measured by fluorescence with terephthalate: (a) the fluorescent spectra in ZnO samples irradiated for 2 h and (b) variation of the amount of  $\cdot\text{OH}$  versus irradiation time under visible light conditions.

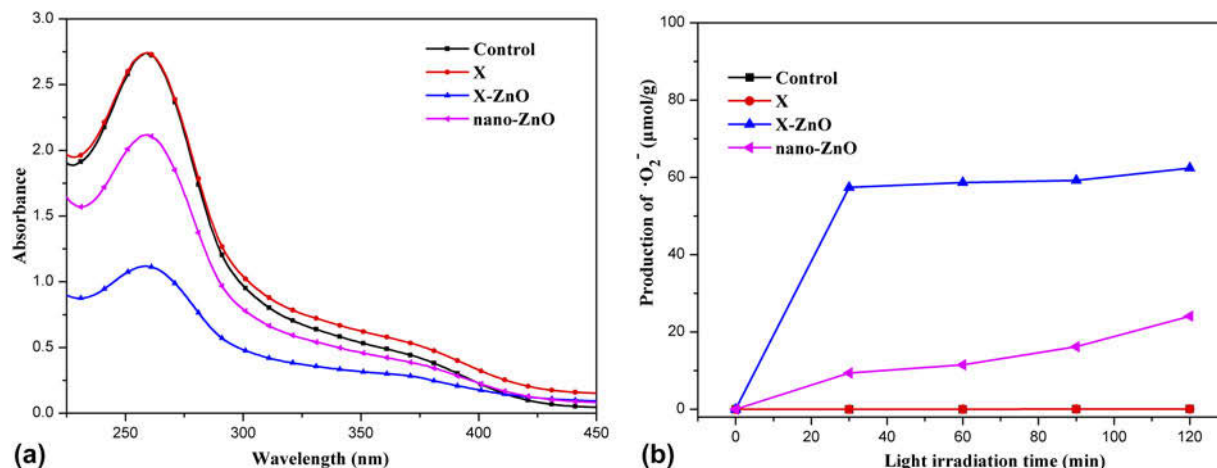


FIG. 7. Production of  $\text{O}_2^-$  in the suspension of ZnO samples measured by UV-vis absorbance with NBT: (a) UV-vis spectra in ZnO samples irradiated for 2 h and (b) variation of the amount of  $\text{O}_2^-$  versus irradiation time in ZnO samples under visible light conditions.

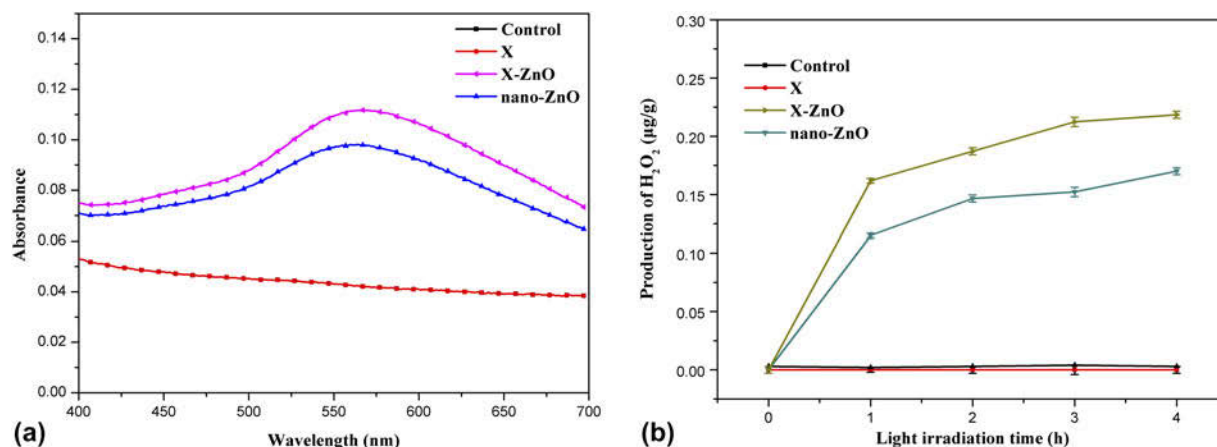


FIG. 8. Production of  $\text{H}_2\text{O}_2$  in the suspension of ZnO samples measured by UV-vis spectra: (a) in ZnO samples irradiated for 2 h and (b) variation of the amount of  $\text{H}_2\text{O}_2$  in ZnO samples versus irradiation time under visible light conditions.

TABLE I. Average concentration of ROS generated by X, X-ZnO, and nano-ZnO.

Particles	$\cdot\text{OH}$ ( $\mu\text{mol}$ )	$\text{O}_2^-$ ( $\mu\text{mol}$ )	$\text{H}_2\text{O}_2$ ( $\mu\text{mol}$ )	Total ( $\mu\text{mol}$ )
X	...	...	...	...
X-ZnO	$0.60 \pm 0.02$	$64.42 \pm 0.60$	$0.22 \pm 0.01$	$65.24 \pm 0.63$
Nano-ZnO	$4.60 \pm 0.02$	$24.10 \pm 0.60$	$0.17 \pm 0.01$	$28.87 \pm 0.63$

ZnO on the surface of zeolite can improve the production content of ROS in ZnO suspension. It was attributed to the fact that the specific surface area of supported ZnO was much higher than that of nano-ZnO, which can provide more available reaction sites for light absorption.<sup>48,49</sup> And Li et al.<sup>31</sup> investigated that there was a linear correlation between the average concentration of total ROS and the antibacterial survival rates. The higher the average concentration of total ROS produced by nanoparticles, the better the antibacterial activities of

nanoparticles were. Thus, X-ZnO has better antibacterial activities than nano-ZnO.

In addition, we understand that some other factors such as ion release may potentially affect the antibacterial activities of ZnO. To determine the ion release effect on the antibacterial activities, we monitored the ion that released from suspensions of X-ZnO and nano-ZnO under 2 h of visible light irradiation (the total concentration of ZnO was 0.48 mg/mL). The concentration of released  $\text{Zn}^{2+}$  ions determined by ICP-AES in the suspensions of X-ZnO and nano-ZnO particles was 4.56 mg/L and 4.26 mg/L, respectively. However, it was reported that the minimum inhibitory of  $\text{Zn}^{2+}$  was 10–20 mg/L.<sup>26</sup> And concentrations of released  $\text{Zn}^{2+}$  ions from X-ZnO and nano-ZnO suspensions were much lower than the minimum inhibitory concentration of  $\text{Zn}^{2+}$ . Thus, it is believed that the released  $\text{Zn}^{2+}$  ions were not the primary factor for the antimicrobial activities of ZnO.

#### IV. CONCLUSION

In this article, ZnO with layer-like morphology was prepared using 13X zeolite as a support. The results of the OD test and plate counting method suggest that pure zeolite (X) almost had no antimicrobial abilities, both X-ZnO and nano-ZnO showed obvious antimicrobial activities against *E. coli* and *S. aureus*. In addition, the ZnO supported on the surface of zeolite had higher antimicrobial activities than nano-ZnO particles under visible light conditions, especially against *E. coli*. The average concentration of total ROS under visible light conditions released from X-ZnO aqueous suspension was much higher than that of nano-ZnO aqueous suspension. It was attributed to the fact that the supported ZnO has much larger specific surface area than nano-ZnO, which can provide more available reaction sites for light absorption. This was the main reason for X-ZnO that had better antibacterial activities than nano-ZnO. It is an effective method to improve the antimicrobial activities of ZnO under visible light conditions by supporting X-ZnO.

#### ACKNOWLEDGMENTS

The authors thank the financial support of the Natural Science Foundation of China (Grants Nos. 51173208 and 51373202) and the Science Foundation of Guangdong Province (Grant No. S2011020001212). They thank the open project of Guangdong Provincial Key Laboratory of High Performance Resin-based Composites for the provided support.

#### REFERENCES

- P.J.P. Espitia, N.F.F. Soares, J.S.R. Coimbra, N.J. de Andrade, and E.A.A. Medeiros: Zinc oxide nanoparticles: Synthesis, antimicrobial activity and food packaging applications. *Food Bioprocess Technol.* **5**, 1447 (2012).
- J. Sawai: Quantitative evaluation of antibacterial activities of metallic oxide powders (ZnO, MgO, and CaO) by conductimetric assay. *J. Microbiol. Methods* **54**, 177 (2003).
- M. Rai, A. Yadav, and A. Gade: Silver nanoparticles as a new generation of antimicrobials. *Biotechnol. Adv.* **27**, 76 (2009).
- E.L. Bradley, L. Castle, and Q. Chaudhry: Applications of nanomaterials in food packaging with a consideration of opportunities for developing countries. *Trends Food Sci. Technol.* **22**, 604 (2011).
- N. Cioff, L. Torsi, N. Ditaranto, G. Tantillo, L. Ghibelli, L. Sabbatini, T. Bleve-Zacheo, M. D'Alessio, P.G. Zambonin, and E. Traversa: Copper nanoparticle/polymer composites with antifungal and bacteriostatic properties. *Chem. Mater.* **17**, 5255 (2005).
- L.K. Adams, D.Y. Lyon, and P.J.J. Alvarez: Comparative ecotoxicity of nanoscale TiO<sub>2</sub>, SiO<sub>2</sub>, and ZnO water suspensions. *Water Res.* **40**, 3527 (2006).
- K.M. Reddy, K. Feris, J. Bell, D.G. Wingett, C. Hanley, and A. Punnoose: Selective toxicity of zinc oxide nanoparticles to prokaryotic and eukaryotic systems. *Appl. Phys. Lett.* **90**, 213902 (2007).
- T. Gordon, B. Perlstein, O. Houbara, I. Felner, E. Banin, and S. Margel: Synthesis and characterization of zinc/iron oxide composite nanoparticles and their antibacterial properties. *Colloids Surf., A* **374**, 1 (2011).
- D. Yan, G. Yin, Z. Huang, L. Li, X. Liao, X. Chen, Y. Yao, and B. Hao: Cellular compatibility of biomaterialized ZnO nanoparticles based on prokaryotic and eukaryotic systems. *Langmuir* **27**, 13206 (2011).
- R. Brayner, R. Ferrari-Iliou, N. Brivois, S. Djediat, M.F. Benedetti, and F. Fiévet: Toxicological impact studies based on *Escherichia coli* bacteria in ultrafine ZnO nanoparticles colloidal medium. *Nano Lett.* **6**, 866 (2006).
- T. Ohira, O. Yamamoto, Y. Iida, and Z. Nakagawa: Antibacterial activity of ZnO powder with crystallographic orientation. *J. Mater. Sci.: Mater. Med.* **19**, 1407 (2008).
- M. Premanathan, K. Karthikeyan, K. Jeyasubramanian, and G. Manivannan: Selective toxicity of ZnO nanoparticles toward Gram-positive bacteria and cancer cells by apoptosis through lipid peroxidation. *J. Nanomed. Nanotechnol.* **7**, 184 (2011).
- Y. Xie, Y. He, P.L. Irwin, T. Jin, and X. Shi: Antibacterial activity and mechanism of action of zinc oxide nanoparticles against campylobacter jejuni. *Appl. Environ. Microbiol.* **77**, 2325 (2011).
- L. Zhang, J. Jiang, Y. Ding, M. Povey, and D. York: Investigation into the antibacterial behaviour of suspensions of ZnO nanoparticles (ZnO nanofluids). *J. Nanopart. Res.* **9**, 479 (2007).
- N. Jones, B. Ray, K.T. Ranjit, and A.C. Manna: Antibacterial activity of ZnO nanoparticle suspensions on broad spectrum of microorganisms. *FEMS Microbiol. Lett.* **279**, 71 (2008).
- H. Yang, C. Liu, D. Yang, H. Zhang, and Z. Xi: Comparative study of cytotoxicity, oxidative stress and genotoxicity induced by four typical nanomaterials: The role of particle size, shape and composition. *J. Appl. Toxicol.* **29**, 69 (2009).
- G. Applerot, A. Lipovsky, R. Dror, N. Perkas, Y. Nitzan, R. Lubart, and A. Gedanken: Enhanced antibacterial activity of nanocrystalline ZnO due to increased ROS-mediated cell injury. *Adv. Funct. Mater.* **19**, 842 (2009).
- K.R. Raghupathi, R.T. Koodali, and A.C. Manna: Size-dependent bacterial growth inhibition and mechanism of antibacterial activity of zinc oxide nanoparticles. *Langmuir* **27**, 4020 (2011).
- X. Xu, D. Chen, Z. Yi, M. Jiang, L. Wang, Z. Zhou, X. Fan, Y. Wang, and D. Hui: Antimicrobial mechanism based on H<sub>2</sub>O<sub>2</sub> generation at oxygen vacancies in ZnO crystals. *Langmuir* **29**, 5573 (2013).
- G.D. Mihai, V. Meynen, M. Mertens, N. Bilba, P. Cool, and E.F. Vansant: ZnO nanoparticles supported on mesoporous MCM-41 and SBA-15: A comparative physicochemical and photocatalytic study. *J. Mater. Sci.* **45**, 5786 (2010).
- X. Chen, Q. Meng, J. Chen, and Y. Long: A facile route to synthesize mesoporous ZSM-5 zeolite incorporating high ZnO loading in mesopores. *Microporous Mesoporous Mater.* **153**, 198 (2012).
- A.A. Alswat, M. Bin Ahmad, T.A. Saleh, M.Z. Bin Hussein, and N.A. Ibrahim: Effect of zinc oxide amounts on the properties and antibacterial activities of zeolite/zinc oxide nanocomposite. *Mater. Sci. Eng., C* **68**, 505 (2016).
- A.A. Alswat, M. Bin Ahmad, and T.A. Saleh: Preparation and characterization of zeolite/zinc oxide-copper oxide nanocomposite: Antibacterial activities. *Colloid Interface Sci. Commun.* **16**, 19 (2017).
- A.A. Alswat, M. Bin Ahmad, M.Z. Hussein, N.A. Ibrahim, and T.A. Saleh: Copper oxide nanoparticles-loaded zeolite and its characteristics and antibacterial activities. *J. Mater. Sci. Technol.* **33**, 889 (2017).
- K. Kasemets, A. Ivask, H.C. Dubourguier, and A. Kahru: Toxicity of nanoparticles of ZnO, CuO, and TiO<sub>2</sub> to yeast *Saccharomyces cerevisiae*. *Toxicol. In Vitro* **23**, 1116 (2009).



26. S.J. Park, Y.C. Park, S.W. Lee, M.S. Jeong, K.N. Yu, H. Jung, J.K. Lee, J.S. Kim, and M.H. Cho: Comparing the toxic mechanism of synthesized zinc oxide nanomaterials by physico-chemical characterization and reactive oxygen species properties. *Toxicol. Lett.* **207**, 197 (2011).
27. T. Xia, M. Kovochich, M. Liang, L. Mädler, B. Gilbert, H. Shi, J.I. Yeh, J.I. Zink, and A.E. Nel: Comparison of the mechanism of toxicity of zinc oxide and cerium oxide nanoparticles based on dissolution and oxidative stress properties. *ACS Nano* **2**, 2121 (2008).
28. M. Li, L. Zhu, and D. Lin: Toxicity of ZnO nanoparticles to *Escherichia coli*: Mechanism and the influence of medium components. *Environ. Sci. Technol.* **45**, 1977 (2011).
29. H. Yin, P.S. Casey, M.J. McCall, and M. Fenech: Effects of surface chemistry on cytotoxicity, genotoxicity, and the generation of reactive oxygen species induced by ZnO nanoparticles. *Langmuir* **26**, 15399 (2010).
30. I. Perelshtein, G. Applerot, N. Perkas, E. Wehrschetz-Sigl, A. Hasmann, G.M. Guebitz, and A. Gedanken: Antibacterial properties of an in situ generated and simultaneously deposited nanocrystalline ZnO on fabrics. *ACS Appl. Mater. Interfaces* **1**, 363 (2009).
31. Y. Li, W. Zhang, J. Niu, and Y. Chen: Mechanism of photo-generated reactive oxygen species and correlation with the antibacterial properties of engineered metal-oxide nanoparticles. *ACS Nano* **6**, 5164 (2012).
32. T. Xia, M. Kovochich, J. Brant, M. Hotze, J. Sempf, T. Oberley, C. Sioutas, J.I. Yeh, M.R. Wiesner, and A.E. Nel: Comparison of the abilities of ambient and manufactured nanoparticles to induce cellular toxicity according to an oxidative stress paradigm. *Nano Lett.* **6**, 1794 (2006).
33. E. Burello and A.P. Worth: A theoretical framework for predicting the oxidative stress potential of oxide nanoparticles. *Nanotoxicology* **5**, 228 (2011).
34. A. Lipovsky, Y. Nitzan, A. Gedanken, and R. Lubart: Antifungal activity of ZnO nanoparticles-the role of ROS mediated cell injury. *Nanotechnology* **22**, 105101 (2011).
35. J. Jiang, G. Li, Q. Ding, and K. Mai: Ultraviolet resistance and antimicrobial properties of ZnO-supported zeolite filled isotactic polypropylene composites. *Polym. Degrad. Stab.* **97**, 833 (2012).
36. M. Li, G. Li, J. Jiang, Y. Tao, and K. Mai: Preparation, antimicrobial, crystallization and mechanical properties of nano-ZnO-supported zeolite filled polypropylene random copolymer composites. *Compos. Sci. Technol.* **81**, 30 (2013).
37. M. Li, G. Li, Y. Fan, J. Jiang, Q. Ding, X. Dai, and K. Mai: Effect of nano-ZnO-supported 13X zeolite on photo-oxidation degradation and antimicrobial properties of polypropylene random copolymer. *Polym. Bull.* **71**, 2981 (2014).
38. X. Xu, Z. Zhou, and W. Zhu: Studies on the active oxygen in zinc oxides with different morphologies. *Mater. Sci. Forum* **610-613**, 229 (2009).
39. X. Xu, X. Duan, Z. Yi, Z. Zhou, X. Fan, and Y. Wang: Photocatalytic production of superoxide ion in the aqueous suspensions of two kinds of ZnO under simulated solar light. *Catal. Commun.* **12**, 169 (2010).
40. P. Schopfer: Histochemical demonstration and localization of H<sub>2</sub>O<sub>2</sub> in organs of higher plants by tissue printing on nitrocellulose paper. *Plant Physiol.* **104**, 1269 (1994).
41. H.A. Sani, M.B. Ahmad, M.Z. Hussein, N.A. Ibrahim, A. Musa, and T.A. Saleh: Nanocomposite of ZnO with montmorillonite for removal of lead and copper ions from aqueous solutions. *Process Saf. Environ. Prot.* **109**, 97 (2017).
42. J. Zhang, L. Sun, J. Yin, H. Su, C. Liao, and C. Yan: Control of ZnO morphology via a simple solution route. *Chem. Mater.* **14**, 4172 (2002).
43. U. Pal and P. Santiago: Controlling the morphology of ZnO nanostructures in a low-temperature hydrothermal process. *J. Phys. Chem. B* **109**, 15317 (2005).
44. H.C. Ong and G.T. Du: The evolution of defect emissions in oxygen-deficient and -surplus ZnO thin films: The implication of different growth modes. *J. Cryst. Growth* **265**, 471 (2004).
45. S.A. Studenikin, N. Golego, and M. Cocivera: Fabrication of green and orange photoluminescent, undoped ZnO films using spray pyrolysis. *J. Appl. Phys.* **84**, 2287 (1998).
46. B. Lin and Z. Fu: Green luminescent center in undoped zinc oxide films deposited on silicon substrates. *Appl. Phys. Lett.* **79**, 943 (2001).
47. K. Vanheusden, W.L. Warren, C.H. Seager, D.R. Tallant, and J.A. Voigt: Mechanisms behind green photoluminescence in ZnO phosphor powders. *J. Appl. Phys.* **79**, 7983 (1996).
48. A. Nel, T. Xia, L. Mädler, and N. Li: Toxic potential of materials at the nanolevel. *Science* **311**, 622 (2006).
49. O. Choi and Z. Hu: Size dependent and reactive oxygen species. *Environ. Sci. Technol.* **42**, 4583 (2008).